# Bandwidth Enhancement of UWB Dual-Polarized Antennas

**Nina Lorho[1, 2, *], William Hubert[1], Sébastien Lestieux[1], Anne Chousseaud[2], and Tchanguiz Razban[2]**

**Abstract**—In this paper, we discuss the impedance and radiation properties of planar UWB (any ultra wide frequency band) dual-polarized antennas. While their performance is usually defined using the impedance bandwidth, some applications require pattern stability over broad frequency bands. An analysis of the behaviour of three UWB dual-polarized antennas (Bowtie Antenna, Toothed Log-Periodic Antenna and Sinuous Antenna) showed interesting conclusions in terms of impedance matching bandwidth and radiation pattern steadiness. Starting from there, we then developed a method that consists in meandering the original structure. This method allows for miniaturization as well as radiation bandwidth enhancement. As a final result, an electrically small antenna with an impedance bandwidth of more than a decade and a steady radiation pattern over it has been developed.

## 1. INTRODUCTION

In the radiofrequency domain, various applications need antennas with an ultra wide bandwidth (at least 500 MHz or a fractional bandwidth of more than 0.2 as defined by the ITU Radiocommunication Sector in [1]). This applies to instance in the case of spectrum monitoring and software-defined radios (SDR). In addition, there has been an ever growing interest in the ultra-wideband technology in the past decades. It is indeed a promising technology because of its low vulnerability to multipath and its reduced probability of detection and interception. In addition, systems using this technology are able to transmit data at high rates and low power. These performances can be obtained using diversity techniques (spatial diversity, polarization diversity, pattern diversity, . . .).

The first concern regarding UWB antennas is the bandwidth. The IEEE standards [2] define the bandwidth of an antenna as the frequency range for which a characteristic (impedance, gain, efficiency, directivity or polarization) is compliant with a given specification. Poor levels of impedance matching limit the antenna efficiency. The later is therefore usually considered to be the most important factor. For this reason, the performance of UWB antennas is often given in terms of "impedance bandwidth". However, while impedance matching can be guaranteed within a given bandwidth, it does not necessarily imply a steady pattern over it. In this case, radiation patterns should be accepted as a best effort, should they be irregular with respect to the angle or the frequency. The impedance matching bandwidth and the radiation bandwidth might therefore be different. This may limit the final frequency range usable by a system.

Some applications however do require specific radiation pattern characteristics (gain, polarization) over a wide impedance matching bandwidth. In some cases, pattern nulls should be avoided because they can cause accuracy issues in measurement applications or any other fault. Other applications may require a dual linearly polarized radiation pattern [3]. It has been proved for instance that the accuracy of short range radars is improved with the use of polarization diversity [4]. It is also of great interest in MIMO systems to increase the data rates along with the channel capacity.

Classic UWB dual-polarized antennas belong to the traveling-wave category. Well-known examples are the Vivaldi antenna or the ridged horn [5]. They exhibit a wide impedance bandwidth (a decade typically) and the pattern is stable over the later bandwidth. But they present directive radiation patterns, not always required depending on the applications, and their size can be troublesome. A decent compromise in terms of size is offered by UWB planar dual-polarized antennas [6].

In this study, we aim to develop planar dual-polarized antennas for any UWB frequency band (their dimensions can be transposed to any frequency band to suit the needs of the given application) with reduced size and enhanced performances in terms of polarization and impedance. The aim is to simultaneously increase both impedance and radiation bandwidths. To achieve this, we developed a novel methodology to enhance the radiation and impedance bandwidths of well-known planar UWB dual-polarized antennas based on their behavior.

Starting from the Bowtie Antenna, we can show that this topology may evolve to form an antenna that presents similar impedance and radiation frequency bandwidths. In addition, this bandwidth can also be widened by decreasing the lower bound of the impedance bandwidth.

In this paper, frequency-dependant characteristics will be displayed as a function of the electrical size $a_{elec}$ rather than the frequency. By doing so, these characteristics can be transposed in the frequency domain to antennas of any size by using the following relations:

$$a_{elec} = \frac{a}{\lambda} = \frac{a \times f}{c} \tag{1}$$

The frequency $f$ is therefore linked to the electrical size by:

$$f = \frac{a_{elec} \times c}{a} \tag{2}$$

where $a$ is the size of the antenna, that is the diameter of the minimum sphere that encloses the antenna; $\lambda$ is the free-space wavelength at the working frequency $f$; $c$ is the speed of light.

## 2. UWB DUAL-POLARIZED MEANDERED ANTENNAS: A CLASS OF PATTERN-CONSISTENT ANTENNAS

### 2.1. Performances of the Bowtie Antenna

For applications using only one linear polarization, dipole-like antennas are optimal. In theory, they present a pure polarization over the whole bandwidth. By extension, thick dipoles are known to increase the matching bandwidth [7]. Eventually, the largest bandwidth is obtained when the antenna presents an optimized transition between the feed and the surrounding medium [7]. This optimal transition is embodied by the Biconical Antenna. For size issues, the Bowtie Antenna is often preferred to the later because of its planar profile.

Bowtie antennas are defined by their outer radius Ro, inner radius Ri and angle $\alpha$ that defines the cone. The outer radius and inner radius are respectively responsible for the lower frequency of operation and the higher frequency of operation. The dual-polarized version of the Bowtie obeys the principles defined in [8]. A second element, identical to the first one but rotated by 90°, is added. As a consequence, an orthogonal polarization is implemented while the cross-polarization remains low.

As angle $\alpha$ increases, the input impedance of the antenna becomes stabilized over a wider bandwidth. An optimum is reached at $\alpha = 45°$ (Fig. 1) and the 10 dB-impedance matching is achieved starting at an electrical size of $\lambda$. The antenna becomes self-complementary. According to [9], this configuration is optimal in terms of bandwidth.

We performed various simulations on the Bowtie Antenna (Figs. 2 and 3). These indicate that irregularities on the radiation pattern appear when the antenna electrical size exceeds $\lambda$ even though a good level of matching is obtained. At the same time, the on-axis gain for the co-polarization experiences a drastic drop (more than 10 dB, Fig. 3). This default can be explained by the emergence of higher order modes along the structure of the antenna: current nulls appear along the structure which results in a distorted radiation pattern. It is however important to note that the cross-polarization remains at a low level throughout the whole frequency band (the cross-polarization rejection reaches 20 dB). The impedance bandwidth of a self-complementary dual-polarized Bowtie Antenna reaches 10 : 1 while the radiation bandwidth reaches 2 : 1.
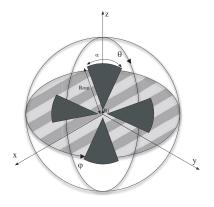
**Figure 1.** Dual-polarized Bowtie Antenna. The circle represents the azimuthal plane ($\theta = 90°$).
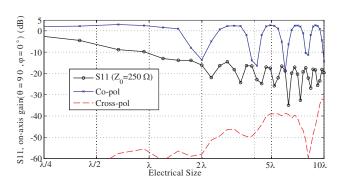


**Figure 2.** Impedance matching and on-axis gain variation w.r.t the electrical size.
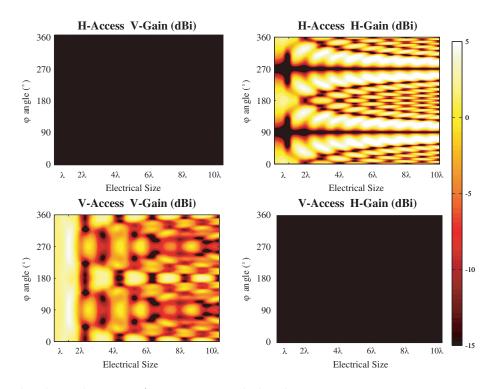


**Figure 3.** Dual-polarized Bowtie Antenna azimuthal radiation pattern.

While this antenna offers an interesting alternative in terms of bulk, our analysis shows that it might not be suitable for applications that require pattern stability over an ultra-wide bandwidth, such as 10 : 1.

## 2.2. From the Bowtie Antenna to the Toothed Log-Periodic Antenna

The Toothed Log-Periodic Antenna belongs to the category of planar multi-resonant antennas. In this discussion, we believe that it is relevant to consider these antennas as meandered evolutions of the Bowtie. This antenna has been introduced in 1958 by Duhamel [10]. Periodical discontinuities that consist of teeth are introduced alternately and periodically on each side of the classic dual-polarized Bowtie as shown in Fig. 4.

Those periodical discontinuities are spread along the radius of the structure using a log-periodic

expansion:

$$R_{n+1} = R_n \times \tau \tag{3}$$

where $R_n$ is the radius of the $n$-th periodic discontinuity, and $\tau$ is the expansion factor that defines the width of the teeth. The angular expansion $\beta$ is responsible for the length of each tooth.

### 2.2.1. Similarities and Differences with the Bowtie Antenna

Figure 4 depicts dual-polarized TLPAs where the number of periodical discontinuities $(N)$ is 15, and the expansion factor $\tau$ is 0.75. The last antenna on the right has an angular width $\beta$ of 40°. As shown in Fig. 5, the TLPA achieves a 10 dB-return loss impedance matching at a slightly smaller electrical size $(0.75\lambda)$ as compared to the Bowtie $(\lambda)$. As for the impedance bandwidth, the later is improved on the TLPA because its lower bound is decreased. No major change is noticed on the higher end of the impedance bandwidth. Fig. 6 shows the on-axis gain for both the Bowtie and the TLPA. It is displayed for only one access as the behaviour is completely symmetric for both access regarding the on-axis gain $(\theta = 90°, \varphi = 0°)$. A similar gain-drop is also experienced when the antenna is electrically small. On the TLPA however, the gain-drop happens for an electrical size of $\lambda/2$ which is half that of the electrical size of the Bowtie $(\lambda)$ at the gain-drop.

It is also important to notice a major difference between these two antennas. Throughout the whole frequency band, the cross-polarization of the Bowtie remains low (Figs. 2 and 3). The vertical (resp. horizontal) element is responsible for the vertical (resp. horizontal) polarization. On the TLPA however, the co-polarization rapidly increases before the gain drop. As can be seen on Fig. 7, the vertical (resp. horizontal) polarization is principal for the vertical (resp. horizontal) access (i.e., the vertical (resp. horizontal) antenna element) when the antenna size is smaller than $\lambda/2$. For these electrical sizes, the TLPA radiation pattern behaviour still follows that of the Bowtie: omnidirectional for the vertical polarization and bi-directional for the horizontal polarization. After the gain drop (i.e., the antenna electrical size exceeds $\lambda/2$), the horizontal (resp. vertical) polarization becomes principal for the vertical (resp. horizontal) element. It remains steady afterwards over a 10:1 bandwidth. This phenomenon will be further referred to as the "polarization inversion" and has been noticed for the first time by the
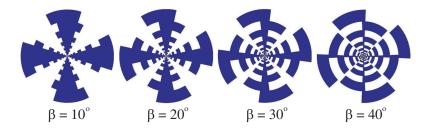


$\beta = 10°$       $\beta = 20°$       $\beta = 30°$       $\beta = 40°$

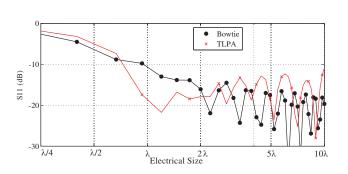**Figure 4.** Dual-polarized Toothed Log-Periodic Antenna construction.



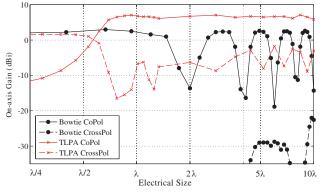**Figure 5.** Impedance matching comparison between the Bowtie and the TLPA.

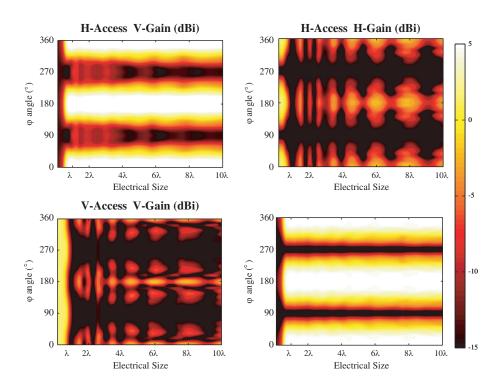**Figure 6.** On-axis gain comparison between the Bowtie and the TLPA.

**Figure 7.** Dual-polarized TLPA azimuthal radiation pattern ($N = 15$, $\beta = 40°$).

authors in [11] on the Sinuous Antenna. It implies that the cross-polarization becomes principal when the antenna electrical size is bigger than $\lambda/2$.

An explanation for the polarization inversion lies in the fact that the periodical discontinuities generate the orthogonal polarization to that of the original Bowtie. The original Bowtie can only generate a limited amount of cross-polarization as it is a symmetric and differentially-fed antenna. However, if orthogonal and asymmetric elements are introduced along the structure, currents can propagate along those newly created paths. As those paths are asymmetric, the generated field do not cancel out each other and therefore generate the orthogonal polarization. When the size of the periodical discontinuities is of the same order of magnitude as the wavelength, the energy is no longer coupled to the principal polarization, resulting in the polarization inversion.

### 2.2.2. Behaviour Analysis

In this section, an analysis will be conducted on the two major parameters that differentiate the TLPA from the Bowtie Antenna: the number of meandered sections (or periodical discontinuities, $N$) and the angular expansion of these sections ($\beta$). This analysis will then lead to conclusions on the TLPA behaviour.

*Variation of the number of meandered sections $N$*  The multi-resonant behaviour of the TLPA appears as the number of arms ($N$) increases (Figs. 8 and 9). When $N$ is low, the impedance bandwidth is restricted (hardly 6 : 1), and gain variations of the order of 10 dB happen for both the co-polarization and the cross-polarization throughout the impedance bandwidth. As $N$ increases, frequency repetitive patterns appear throughout the frequency band. These multiple resonances enhance the impedance bandwidth to reach 10 : 1. Another important consequence is that the radiation pattern shows the same behaviour. Less irregularity for the co-polarization is obtained (of the order of 2 dB) and better cross-polarization rejection (close to 10 dB) is achieved. This is a drastic change as compared to the Bowtie Antenna: radiation patterns are no longer subject to higher order modes and can therefore become steady over a wide bandwidth (10 : 1). There is however no evidence of the impact of $N$ on the
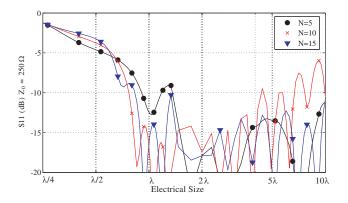
**Figure 8.** Dual-polarized TLPA input reflection coefficient (parameter: $N$, $\beta = 40°$, $\tau = 0.75$).



**Figure 9.** Dual-polarized TLPA on-axis gain (parameter: $N$, $\beta = 40°$, $\tau = 0.75$). Solid line: co-polarization; Dashed line: cross-polarization.
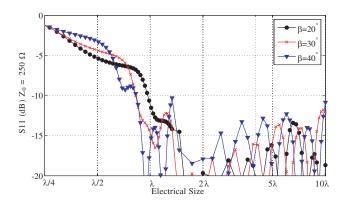


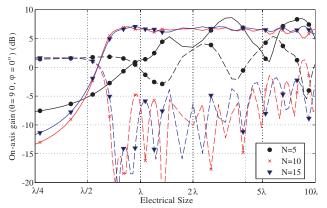**Figure 10.** Dual-polarized TLPA input reflection coefficient (parameter: $\beta$, $N = 15$, $\tau = 0.75$).
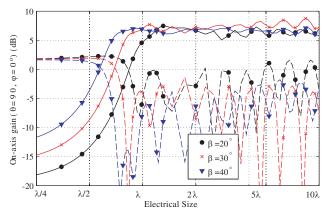


**Figure 11.** Dual-polarized TLPA on-axis gain (parameter: $\beta$, $N = 15$, $\tau = 0.75$). Solid line: co-polarization; Dashed line: cross-polarization.

polarization inversion: the electrical size at which this phenomenon happens remains the same as $N$ increases.

*Variation of the angular expansion $\beta$*   When $\beta$ increases, the lowest frequency of the impedance bandwidth decreases (Fig. 10). At the same time, the polarization inversion happens for lower electrical sizes (Fig. 11). Indeed, the meandered arms resonate at lower frequencies as their lengths increase, resulting in a smaller electrical size.

### 2.2.3. Conclusions on the TLPA Impedance and Radiation Bandwidths

The periodical discontinuities prevent the arising of unwanted higher order modes which helps to keep the pattern steady (when $a/\lambda \geq 1$) and they have a miniaturizing effect on the antenna (about 30%). The two major parameters $N$ and $\beta$ respectively have an impact on the radiation pattern steadiness and the lower bound of both the impedance and radiation bandwidth. In the end, the TLPA is able to achieve a $10:1$ bandwidth regarding both the impedance matching and the radiation pattern stability. When $N$ and $\beta$ are high (for instance $\beta = 40°$ and $N = 15$), frequency-independent characteristics are obtained. The $10\,\mathrm{dB}$ return-loss is achieved at an electrical size of $0.83\lambda$, and the polarization inversion happens at an electrical size of approximately $0.57\lambda$. Both radiation and impedance bandwidths therefore overlap

thus making the TLPA an interesting alternative to the Bowtie Antenna. However, the cross-polarization rejection can be troublesome.

## 2.3. From the Toothed Log-Periodic Antenna to the Sinuous Antenna

In 1987, the same author introduces the Sinuous Antenna [12]. The curves of the antenna are drawn using the following equations in polar coordinates:

$$R_t \times \tau^N \leq t \leq R_t \tag{4}$$

$$R = t \tag{5}$$

$$\varphi = \alpha \times \frac{\pi}{180} \times \sin\left(\frac{\pi \times \ln\left(\dfrac{t}{R_t}\right)}{\ln(\tau)}\right) \pm \delta \tag{6}$$

$$\theta = 90° \tag{7}$$

where $R_t$ is the outer radius of the structure, $\alpha$ the angular expansion, $\delta$ the angular width, $\tau$ the expansion factor and $N$ the number of meandered sections.

### 2.3.1. Behaviour Analysis

The Sinuous Antenna is indeed a meandered evolution of the Bowtie (Fig. 12): the sinus function modulates its outer edges to create the periodical discontinuities. It can also be seen as an evolution of the TLPA: the periodical discontinuities are smoothed out (Fig. 13). This makes the impedance and radiation pattern more stable as compared to the Toothed Log-Periodic antenna, as shown in Figs. 14. and 15. In this section, various simulations are carried out on the Sinuous Antenna in order to identify the radiation mechanisms of this antenna.

*Variation of the number of meandered sections $N$* As the number of meandered sections $N$ increases, the same frequency repetitive patterns that were previously noticed on the TLPA appear on the Sinuous Antenna. The lower bound of the impedance matching bandwidth is decreased (Table 2), and a stable 10 dB return-loss match is achieved until an electrical size of $10\lambda$. As for the radiation pattern (Fig. 16),
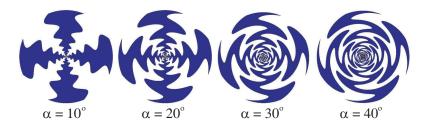


$\alpha = 10°$  $\alpha = 20°$  $\alpha = 30°$  $\alpha = 40°$

**Figure 12.** Dual-polarized Sinuous Antenna construction.



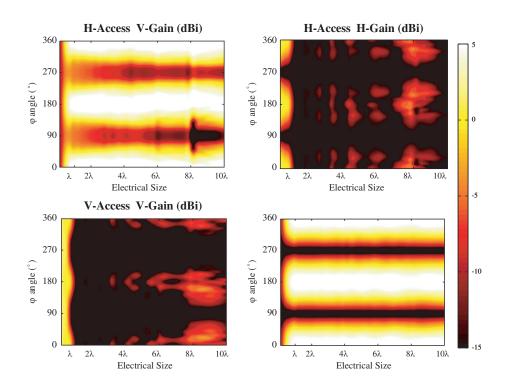**Figure 13.** Evolution from the Toothed Log-Periodic Antenna (Gray) to the Sinuous Antenna (Black).

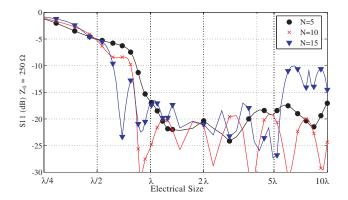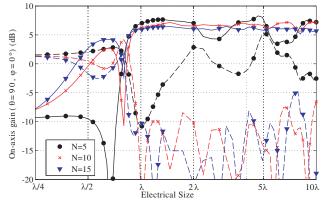**Figure 14.** Dual-polarized Sinuous Antenna azimuthal radiation pattern ($N = 15$, $\alpha = 40°$).



**Figure 15.** Dual-polarized Sinuous Antenna input reflection coefficient (parameter: $N$, $\alpha = 40°$, $\tau = 0.75$).

**Figure 16.** Dual-polarized Sinuous Antenna on-axis gain (parameter: $N$, $\alpha = 40°$, $\tau = 0.75$). Solid line: co-polarization; Dashed line: cross-polarization.

similar conclusions to those concerning the TLPA can be drawn: as $N$ increases, the radiation pattern becomes steady over a 10 : 1 bandwidth after the polarization inversion.

*Variation of the angular expansion $\alpha$*   As angle $\alpha$ increases, the lower bound of the impedance matching bandwidth decreases, resulting in a smaller electrical size and enhanced bandwidth. The co-polarized gain drops while the cross-polarized gain rises to become principal. The cross-polarization rejection increases as the angular expansion of the meandered lines increases to reach approximately 15 dB when $\alpha = 40°$. Similar conclusions can be drawn for both the TLPA and the Sinuous Antenna: periodical discontinuities along the antenna induce multi-resonances that enhance the impedance matching bandwidth.
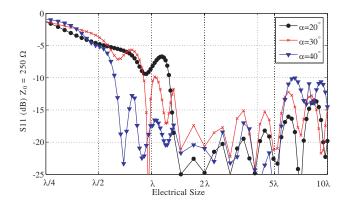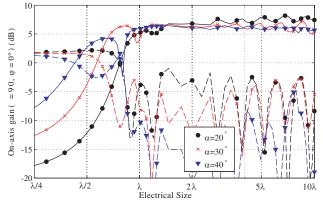
**Figure 17.** Dual-polarized Sinuous Antenna input reflection coefficient (parameter: $\alpha$, $N = 15$, $\tau = 0.75$).



**Figure 18.** Dual-polarized Sinuous Antenna on-axis gain (parameter: $\alpha$, $N = 15$, $\tau = 0.75$). Solid line: co-polarization; Dashed line: cross-polarization.

**Table 1.** TLPA impedance bandwidth and polarization inversion.

| Parameter | Impedance Bandwidth | | | Polarization inversion |
|---|---|---|---|---|
| | Lower bound | Upper bound | Bandwidth | |
| $N = 5$, $\beta = 40°$ | $0.9\lambda$ | $10\lambda$ | **11 : 1** | $0.9\lambda$ |
| $N = 10$, $\beta = 40°$ | $0.77\lambda$ | $10\lambda$ | **9 : 1** | $0.57\lambda$ |
| $N = 15$, $\beta = 40°$ | $0.83\lambda$ | $10\lambda$ | **12 : 1** | $0.57\lambda$ |
| $\beta = 20°$, $N = 15$ | $0.96\lambda$ | $10\lambda$ | **10 : 1** | $0.82\lambda$ |
| $\beta = 30°$, $N = 15$ | $0.83\lambda$ | $10\lambda$ | **12 : 1** | $0.69\lambda$ |
| $\beta = 40°$, $N = 15$ | $0.83\lambda$ | $10\lambda$ | **12 : 1** | $0.57\lambda$ |

**Table 2.** Sinuous antenna impedance bandwidth and polarization inversion.

| Parameter | Impedance Bandwidth | | | Polarization inversion |
|---|---|---|---|---|
| | Lower bound | Upper bound | Bandwidth | |
| $N = 5$, $\beta = 40°$ | $0.83\lambda$ | $10\lambda$ | **12 : 1** | $0.8\lambda$ |
| $N = 10$, $\beta = 40°$ | $0.78\lambda$ | $10\lambda$ | **12.8 : 1** | $0.85\lambda$ |
| $N = 15$, $\beta = 40°$ | $0.62\lambda$ | $10\lambda$ | **16 : 1** | $0.81\lambda$ |
| $\beta = 20°$, $N = 15$ | $1.25\lambda$ | $10\lambda$ | **8 : 1** | $0.77\lambda$ |
| $\beta = 30°$, $N = 15$ | $0.9\lambda$ | $10\lambda$ | **11 : 1** | $0.59\lambda$ |
| $\beta = 40°$, $N = 15$ | $0.62\lambda$ | $10\lambda$ | **16:1** | $0.81\lambda$ |

*2.3.2. Low-Frequency Behaviour of the Sinuous Antenna*

A zoom on the low frequency characteristics (Fig. 19) shows that there is a frequency range for which the cross-polarization levels of the Sinuous Antenna are high (of the order of less than 5 dB). This frequency range corresponds to electrical sizes comprised between $\lambda/4$ and $3\lambda/4$. However, the Sinuous Antenna impedance matching bandwidth starts at approximately $0.6\lambda$. Therefore, the radiation and impedance bandwidths do not overlap.
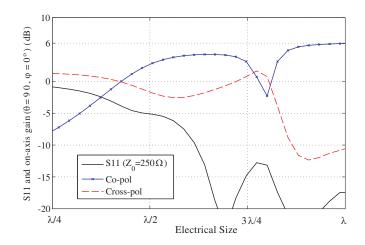
**Figure 19.** Low-frequency (electrical size) behaviour of the Sinuous Antenna ($\alpha = 40°$, $\delta = 22.5°$, $N = 15$, $\tau = 0.75$).

## 2.4. Advantages and Disadvantages of the Toothed Log-Periodic Antenna and the Sinuous Antenna

This section has led to a comparative analysis of low-profile planar UWB dual-polarized antennas. Impedance bandwidths have been increased using periodical discontinuities added to the original structure (Bowtie Antenna).

Those periodical discontinuities have led to two well-known UWB dual-polarized antennas: the Toothed Log-Periodic Antenna and the Sinuous Antenna.

The analysis of the Toothed Log-Periodic Antenna shows interesting performances in terms of impedance bandwidth $(10 : 1)$ and radiation bandwidth $(10 : 1)$ (Table 1, Figs. 20 and 21). Both overlap making this antenna a suitable candidate for applications that require pattern stability, dual polarization and impedance matching over large bandwidths. However, the cross-polarization rejection of this antenna remains poor.

As for the Sinuous Antenna, our study shows that the impedance bandwidth reaches $16 : 1$ (Table 2, Figs. 20 and 21). For low electrical sizes however, our results indicate that the cross-polarization is relatively high. The radiation bandwidth of this antenna still reaches $10 : 1$. Both bandwidths do not overlap because of the low frequency behaviour of this antenna. At higher frequencies, the cross-polarization levels of the Sinuous Antenna are however more interesting than those of the Toothed Log-Periodic Antenna ($15\,\text{dB}$ as compared to less than $10\,\text{dB}$).
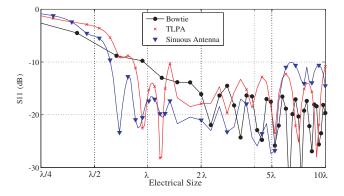


**Figure 20.** Impedance matching comparison among the Bowtie, the TLPA and the Sinuous Antenna.
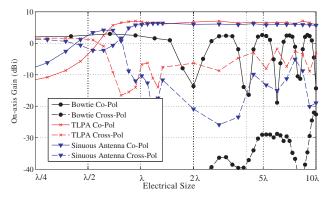


**Figure 21.** On-axis gain comparison among the Bowtie, the TLPA and the Sinuous Antenna.

The initial problematic of this paper is to design a planar UWB dual-linearly polarized antenna with identical impedance and radiation bandwidths. Regarding the later, we tend to believe that the Sinuous Antenna is a good candidate, provided that its low frequency characteristics are improved.

## 3. ANTENNA MEANDERING: A SOLUTION FOR BANDWIDTH IMPROVEMENT OF UWB DUAL-POLARIZED ANTENNAS

In order to improve the low frequency radiation characteristics of the Sinuous Antenna, we propose an approach based on meandering (Fig. 22). A similar approach has been proposed for miniaturizing the TLPA in [13] but, to the best of our knowledge, this technique has not been applied to the Sinuous Antenna, and there is no track of any further analysis of this technique's effects on antennas' radiation properties. Meandering consists in reshaping the antenna in order to lengthen the metallic paths and therefore increase the length of the current paths within the antenna. As the Sinuous Antenna is defined by a curve, meandering is implemented using a modified curve. Eq. (9) is identical to Eq. (5) except that a cosinus function modulates the radius $R(t)$.

$$R_t \times \tau^N \leq t \leq R_t \tag{8}$$

$$R = t \times (1 + r_p \times \cos(\xi \times \varphi(t))) \tag{9}$$

$$\varphi = \alpha \times \frac{\pi}{180} \times \sin\left(\frac{\pi \times \ln\left(\frac{t}{R_t}\right)}{\ln(\tau)}\right) \pm \delta \tag{10}$$

$$\theta = 90° \tag{11}$$



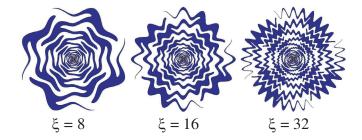$$\xi = 8 \qquad \xi = 16 \qquad \xi = 32$$

**Figure 22.** Dual-polarized Meandered Sinuous Antenna with a variation of the number of meanders $\xi$ and $r_p = 0.1$.
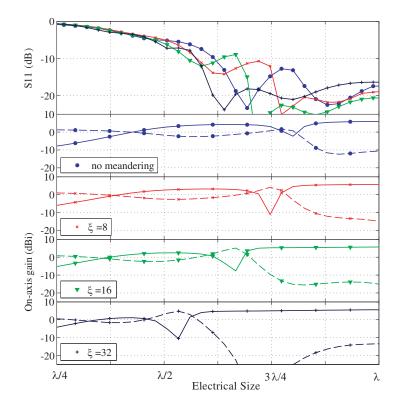
### 3.1. Simulations Results

The parameters for the sinuous curve are $R_t$ (outer radius of the structure), $\alpha$ (angular expansion), $\delta$ (angular width), $\tau$ (expansion factor) and $N$ (number of meandered sections).

The parameters for the curve meandering are $r_p$ (relative amplitude of the meandering curve) and $\xi$ (number of meanders). The Sinuous Antenna design parameters are $N = 15$, $\alpha = 40°$, $\delta = 22.5°$ and $\tau = 0.75$.

#### 3.1.1. Behaviour Analysis: Variation of the Number of Meanders $\xi$

In this section, the effect of the number of meanders $\xi$ will be evaluated on the Sinuous Antenna. As a first assumption, one can think that an increase in the number of meanders might have a shifting effect on the low-frequency characteristics (miniaturization as well as radiation properties) because increasing this number lengthens the metallic paths and therefore leads to greater electrical distances, even though the global antenna size is kept constant.

Figure 23 shows the effect of the design curve meandering on the Sinuous Antenna impedance and radiation characteristics. There is a clear effect of the meanders number $\xi$ on the polarization inversion.

**Figure 23.** Low-frequency effects of curve meandering on the Sinuous Antenna (Parameter: $\xi$, $\alpha = 40°$, $\delta = 22.5°$, $N = 15$, $\tau = 0.75$ and $r_p = 0.1$) impedance (top) and radiation (bottom). Solid line: co-polarization; Dashed line: cross-polarization.

**Table 3.** Meandered sinuous antenna impedance bandwidth and polarization inversion.

| Parameter | Impedance Bandwidth | | Bandwidth | Polarization inversion |
|---|---|---|---|---|
| | Lower bound | Upper bound | | |
| no meander | $0.62\lambda$ | $10\lambda$ | **16 : 1** | $0.81\lambda$ |
| $\xi = 8$, $r_p = 0.1$ | $0.57\lambda$ | $10\lambda$ | **17 : 1** | $0.77\lambda$ |
| $\xi = 16$, $r_p = 0.1$ | $0.56\lambda$ | $10\lambda$ | **18 : 1** | $0.69\lambda$ |
| $\xi = 32$, $r_p = 0.1$ | $0.56\lambda$ | $10\lambda$ | **18 : 1** | $0.56\lambda$ |
| $r_p = 0.1$, $\xi = 16$ | $0.56\lambda$ | $10\lambda$ | **18 : 1** | $0.69\lambda$ |
| $r_p = 0.2$, $\xi = 16$ | $0.51\lambda$ | $10\lambda$ | **20 : 1** | $0.65\lambda$ |

As $\xi$ increases, the polarization inversion happens for lower electrical sizes (i.e., lower frequencies). The lowest electrical size of the impedance matching bandwidth also decreases as compared to the antenna without meandering (a shift of about 10%). However, the results show no influence of the meanders number $\xi$ on the later: a meandered antenna has therefore a lower electrical size as compared to a non-meandered one but it is not the meanders number that has an impact on the lowest bound of the impedance bandwidth. In Table 3, those values are summarized. It appears that an overlapping impedance and radiation bandwidth is achieved when $\xi = 32$. The bandwidth is hence 18:1 while the cross-polarization rejection remains high (15 dB) and pattern stability is achieved throughout that frequency range (Fig. 26).

This analysis partly verifies our first assumption regarding a shift in the low-frequency characteristics of the Sinuous Antenna. Indeed, an increase in $\xi$ slightly miniaturizes the antenna (about 10%) and it shifts the polarization inversion towards lower frequencies.

*3.1.2. Behaviour Analysis: Variation of the Relative Amplitude of the Meandering Curve $r_p$*

In this paragraph, the effect of the relative amplitude of the meanders $\xi$ will be analysed.

Figure 24 shows the effects of the design curve meandering on the Sinuous Antenna and the effects on its characteristics are depicted in Fig. 25. As its relative amplitude $r_p$ increases from 0.1 to 0.2, the lowest electrical size of the impedance matching bandwidth decreases ($0.56\lambda$ to $0.51\lambda$, about 10%). The effect is however smaller on the polarization inversion. The later decreases from $0.69\lambda$ to $0.65\lambda$ (about 5%).
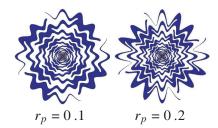


$r_p = 0.1$          $r_p = 0.2$

**Figure 24.** Dual-polarized Meandered Sinuous Antenna with a variation of the relative ampitude of the meandering curve $r_p$ and $\xi = 16$.
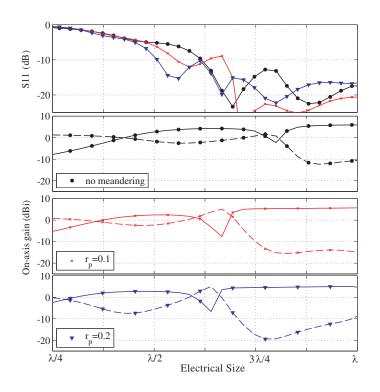


**Figure 25.** Low-frequency effects of curve meandering on the Sinuous Antenna (Parameter: $r_p$, $\alpha = 40°$, $\delta = 22.5°$, $N = 15$, $\tau = 0.75$ and $\xi = 16$) impedance (top) and on-axis gain (bottom). Solid line: co-polarization; Dashed line: cross-polarization.

One could think that an increase in the relative amplitude might also have a miniaturizing effect on the Sinuous Antenna because of the increase in the electrical distances within the antenna. Our results show that its miniaturizing effects are not as pronounced as the increase of the number of meanders. When the relative amplitude is multiplied by 2, a 10% shift on the impedance and a 5% shift on the radiation properties is obtained. Furthermore, adverse effects can appear for higher values at higher electrical sizes.
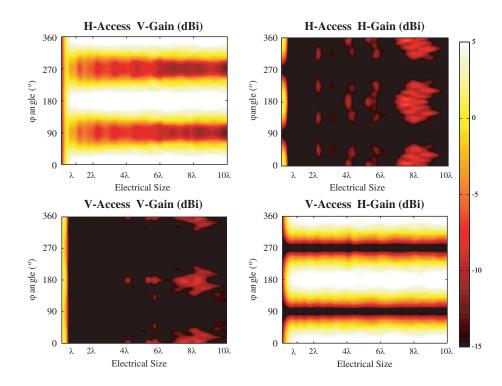
**Figure 26.** Dual-polarized Meandered Sinuous Antenna azimuthal radiation pattern ($\xi = 32$, $r_p = 0.1$).

### 3.1.3. Conclusions on Bandwidth Enhancement of Meandered Sinuous Antennas

In this section, we introduce a sinusoidal meandering of the Sinuous Antenna design curve. Two main parameters define the curve meandering: the number of meanders $\xi$ and the relative amplitude $r_p$. The first parameter has an impact on the polarization inversion while the second is responsible for antenna miniaturization.

It is therefore possible to achieve a smaller antenna that implements the dual-polarization in a planar form. The radiation pattern is steady and purely polarized over a 20 : 1 bandwidth and the later overlaps with the impedance matching bandwidth.

This method is a step forward in the enhancement of UWB antennas' bandwidth. Both impedance and radiation bandwidths have been greatly enhanced from 10 : 1 to approximately 20 : 1. Most importantly, these bandwidths now overlap, making the antenna completely functional in both ranges.

Some limitations on the pattern might arise at higher electrical sizes if the amplitude of the meandering is too big as compared to the wavelength. As a precaution, it is therefore important to keep the relative amplitude of the meanders at a low level as compared to the antenna size.

### 3.2. Measurement Results

In order to verify our assumptions, a prototype of Meandered Sinuous Antenna is fabricated and measured. The meandering curve parameters are $\xi = 32$ and $r_p = 0.1$ because these values have led to an overlapping impedance and radiation bandwidth in the simulations. The design parameters are summed up in Table 4 and the prototype is depicted in Fig. 27. This antenna is then measured from 1 GHz to 8 GHz (therefore leading to electrical sizes shown in this study between $0.25\lambda$ and $\lambda$) using a CMS-balun that performs both impedance transformation (from $250\,\Omega$ to $50\,\Omega$) and mode balancing.

The prototype needs a substrate slab for mechanical handling issues. The relative permittivity of the substrate $\epsilon_r$ as well as its thickness $h$ therefore has an impact on the antenna characteristics. This effect is shown on Fig. 28 where simulations with and without substrate are compared to the measurement which is done with the use of a substrate. Both impedance and radiation characteristics are shifted by a factor 1.25. This factor can be linked to the relative permittivity of the substrate. The

**Table 4.** Antenna prototype design parameters.

| Sinuous Antenna Design Parameters | | | | | Meandering Parameters | | Substrate Parameters | |
|---|---|---|---|---|---|---|---|---|
| $\alpha$ | $\delta$ | $\tau$ | $N$ | $R_t$ | $\xi$ | $r_p$ | $\epsilon_r$ | $h$ |
| 45° | 22.5° | 0.75 | 15 | 2 cm | 32 | 0.1 | 2.55 | 1.6 mm |



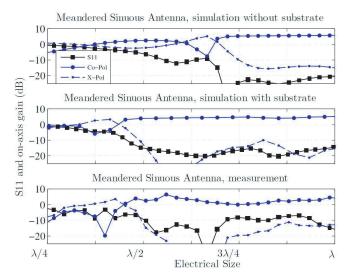**Figure 27.** Dual-polarized Meandered Sinuous Antenna prototype (printed on both sides of the substrate).



**Figure 28.** Simulation and measurement results for the Meandered Sinuous Antenna ($\xi = 32$, $r_p = 0.1$, $\tau = 0.75$, $N = 15$, $\alpha = 45°$, $\delta = 22.5°$).

antenna is neither completely in the air nor enclosed in an electrically large piece of dielectric. The impact of the dielectric is therefore slightly smaller than the square-root of the relative permittivity ($\sqrt{2.55} \approx 1.58$).

The Simulated Antenna with substrate has its impedance matching bandwidth starting at an electrical size of $0.45\lambda$ which corresponds to that of the polarization inversion. The Measured Antenna exhibits the same electrical size concerning the polarization inversion but the lower bound of the impedance bandwidth is slightly bigger at $0.5\lambda$. Higher values of return-loss inside the bandwidth are also noticed. The gap between simulations and measurement results is thus quite small (of the order of 10%). We however believe that these differences are due to the feeding structure's own return loss characteristics.

As for the concerns regarding pattern stability and cross-polarization rejection, the Measured Antenna shows more ripple in the co-polarized gain (the ripple reached 5 dB). The impact of the feeding board at the back of the antenna should be suspected here as well as it represents a large metallic presence in the immediate vicinity of the radiating element. The cross-polarization rejection ratio still remains high with no less than 10 dB and usually more than 15 dB. On Fig. 29, the simulated efficiency and peak total gain is depicted. After an electrical size of $0.43\lambda$, efficiencies higher than 80% and reaching out to 96% are achieved. As for the total gain, it becomes positive after $0.3\lambda$. Both characteristics therefore show that no trade-off has been made to keep both bandwidth and efficiency high.

In Fig. 30, the azimuthal radiation pattern is shown for the realized antenna. These results should be compared with the ones depicted in Fig. 26. The pattern is dual-polarized with low levels of cross-polarization. For both access, the pattern is bidirectionnal and the on-axis gain reaches 5 dBi. For higher frequencies (i.e., when the electrical size reaches $\lambda$), pattern stability becomes an issue.

## 4. CONCLUSION

In this study, we have investigated radiation and impedance characteristics of planar dual-polarized UWB antennas over large bandwidths. We have shown that classic dipolar structures do not exhibit consistent radiation characteristics over more than one octave bandwidth. Multi-resonant antennas such as the Toothed Log-Periodic Antenna and the Sinuous Antenna yield better results in terms of pattern stability but they suffer from either low cross-polarization ratio (TLPA) or polarization inversion inside the frequency band (Sinuous Antenna). On the Sinuous Antenna, we have thus developed an approach based on meandering that allows for antenna miniaturization as well as shifting the polarization inversion outside of the bandwidth of this antenna. Simulation and measurements results fit. This approach therefore allows for the design of planar dual-polarized UWB antennas (more than one decade) with pattern consistent characteristics and reduced size.

However, maintaining an effort towards impedance bandwidth enhancement has limited interest if the feeding devices are band-limited. Indeed, we have been able to measure the antenna up to an electrical size of $\lambda$ (8 GHz) because the balun's bandwidth did not allow any measurement at higher frequencies. We believe that there is a need for symmetric feeding structures whose bandwidth might reach a decade or more. In the same way, our efforts towards radiation pattern stabilization have been ruined at higher frequencies because of near-field elements that disturb the antenna. It could therefore be interesting to develop structures that decouple the antenna from its environment, particularly at the rear, while keeping a low-profile.

## REFERENCES

1. Recommendation ITU-R SM.1755, "Characteristics of ultra-wideband technology (Questions ITU-R 226/1 and ITU-R 227/1).

2. "IEEE standard for definitions of terms for antennas," *IEEE Std 145-2013 (Revision of IEEE Std 145-1993)*, 1–50, Mar. 2014.

3. Klemp, O., O. Schmitz, and H. Eul, "Polarization diversity analysis of dual-polarized log.-per. planar antennas," *2005 IEEE 16th International Symposium on Personal, Indoor and Mobile Radio Communications*, Vol. 4, 2356–2360, Sep. 2005.

4. Zetik, R., J. Sachs, and R. S. Thoma, "UWB short-range radar sensing — The architecture of a baseband, pseudo-noise uwb radar sensor," *IEEE Instrumentation Measurement Magazine*, Vol. 10, No. 2, 39–45, Apr. 2007.

5. Mallahzadeh, A. R., A. A. Dastranj, and H. R. Hassani, "A novel dual-polarized double-ridged horn antenna for wideband applications," *Progress In Electromagnetics Research B*, Vol. 1, 67–80, Apr. 2008.

6. Adamiuk, G., S. Beer, W. Wiesbeck, and T. Zwick, "Dual-orthogonal polarized antenna for uwb-ir technology," *IEEE Antennas and Wireless Propagation Letters*, Vol. 8, 981–984, 2009.

7. Schantz, H. G., *The Art and Science of Ultra-Wideband Antennas*, Artech House, 2005.

8. Adamiuk, G., L. Zwirello, L. Reichardt, and T. Zwick, "UWB cross-polarization discrimination with differentially fed, mirrored antenna elements," *2010 IEEE International Conference on Ultra-Wideband*, Vol. 1, 1–4, Sep. 2010.

9. Mushiake, Y., "Self-complementary antennas," *IEEE Antennas and Propagation Magazine*, Vol. 34, No. 6, 23–29, Dec. 1992.

10. DuHamel, R. H., "Frequency independant antennas," US Patent 2,985,879, Jul. 4, 1958.

11. Lorho, N., G. Lirzin, A. Chousseaud, T. Razban, A. Bikiny, and S. Lestieux, "Miniaturization of an UWB dual-polarized antenna," *2015 IEEE International Conference on Ubiquitous Wireless Broadband (ICUWB)*, 1–5, 2015.

12. DuHamel, R. H., "Dual polarized sinuous antennas," US Patent 703,042, Apr. 1987.

13. Klemp, O., M. Schultz, and H. Eul, "Miniaturization techniques for logarithmically periodic planar-antennas," *15th IEEE International Symposium on Personal, Indoor and Mobile Radio Communications, 2004. PIMRC 2004*, Vol. 1, 412–416, Sep. 2004.